

A DISCRETE ELEMENT METHOD APPROACH FOR THE PRESERVATION OF THE ARCHITECTURAL HERITAGE AGAINST EXPLOSIONS

F. Masi^{1,2}, I. Stefanou¹, P. Vannucci³, and V. Maffi-Berthier²

¹NAVIER
UMR 8205, École des Ponts, IFSTTAR, CNRS, UPE
Champs-sur-Marne, F-77420, France
e-mail: filippo.masi@enpc.fr, ioannis.stefanou@enpc.fr

²Ingérop Conseil et Ingénierie
Rueil-Malmaison, F-92500, France
e-mail: victor.maffi-berthier@ingerop.com

³LMV
UMR 8100, Université de Versailles et Saint-Quentin
Versailles, F-78035, France
e-mail: paoletto.vannucci@uvsq.fr

Keywords: Blast actions, Masonry structures, Discrete Element Method, Architectural heritage.

Abstract. Most emblematic monumental and historical buildings are masonry structures, made of brick and stone. Assess their response and vulnerability against explosive threats is a crucial issue in the preservation of such architectural assets and their visitors. The investigation of the blast loading response of masonry structures requires a proper modelling approach of the material and the loads arising from an explosion.

Here we propose a Discrete Element Method approach to investigate the fast-dynamic response of planar masonry structures subjected to blast loading. The Discrete Element Method captures the detailed mechanical and geometrical characteristics of masonry as well as the inherent coupling between the in- and out-of-plane motions. Blast loads are applied through an external dynamic library, which accounts for the effect of surface rotation of masonry components due to the pressure load (incident angle effect).

The discrete model is validated through existing experimental tests. The numerical simulations are found to predict with high fidelity the dynamic response and failure of the specimens, corroborating our modelling assumptions. The proposed approach is central to understand the behaviour of masonry structures subjected to blast loading and the influence of the various micro-mechanical material parameters.

1 INTRODUCTION

In the present international context, there is a need for the scientific community and institutions to better assess the threat of explosions meant to destroy civil engineering structures. Emblematic historical and monumental buildings, which have been targeted repeatedly, are often made of brick and stone, for which the prediction of the response to blast loading is particularly challenging. These structures tend to be massive, providing a natural resistance to blast pressure, but also typically have very low tensile strength between bricks or stones, leaving their joints able to open, and rendering them susceptible to collapse.

The investigation of the mechanical behaviour of masonry structures attracts significant scientific research, mostly focusing on the mechanical behaviour under quasi-static and seismic loads. In the last decade, increasing interest was shown in the response and potential damage of masonry structures due to explosive events, such as deliberate and/or accidental blasts and vented explosions from gas leaks, see e.g. [1-6].

Attention was focused on the response of planar masonry structures to blast loads. We refer here to the seminal work of Gabrielsen et al. [7] who first experimentally investigated the response to blast loading of full-scale unreinforced masonry walls with and without development of arching actions. Several experimental campaigns investigated the blast performance of one-way arching masonry walls [1-4, 8-10]. Keys and Clubley [2] investigated the debris distribution and failure pattern of masonry walls subjected to long duration blast loading. More recently, Michaloudis and Gebbeken [4] analysed the response of unreinforced masonry walls constrained to rigid supports subjected to far-field and contact explosions through experimental and numerical investigations.

Several modelling strategies were developed to investigate the dynamic response of masonry structures to explosions. We refer herein to both meso- and macro-scale numerical approaches, see e.g. [4, 10-16].

The Discrete Element Method (DEM) is herein proposed as an accurate and effective modelling strategy for masonry structures subjected to explosions. Blast loads are computed using an external dynamic library which

accounts for the effect of surface rotation of building blocks as well as the evolution in time of their relative distance with respect to the impinging blast wave. Through appropriate validation of the proposed approach with experimental data, we prove that DEM is a reliable tool in predicting the response of masonry structures and their failure to far-field explosions. In such scenarios, the mechanical behaviour of the masonry joints plays a leading role in the overall strength and failure of the structure. Failure within the body of masonry bricks does not occur or is usually negligible, as corroborated by experimental tests [1, 2, 4] as well as by theoretical investigations, see e.g. [17] where it is shown that failure of the building blocks is important only under high compression.

We further investigate the accuracy of a rigid block model under quasi-static and dynamic conditions. Non-deformable blocks may provide inaccurate predictions for the out-of-plane response due to an intrinsic overestimation of the flexural stiffness.

The proposed modelling approach is central to investigate in detail the response and failure of masonry structures subjected to far-field explosions as well as to identify the governing micro-mechanical material parameters. It can be used to conceive appropriate and effective protective devices to help in the preservation of the architectural heritage. The discrete model can further be used to perform full-scale numerical tests focusing on the strength of the structure at varying of the geometry, material parameters, as well as the intensity of the blast loading. Ultimately, our numerical model, relying on a detailed description of the system, offers the possibility to conceive in-scale experiments through the definition of appropriate scaling laws. Notice that performing blast experiments either in reduced or in full scale presents many difficulties [18], due to the nature of the loading action (e.g. need of specialized personnel, risks, measuring devices, repeatability, uncertainties etc.)

The paper is structured as follows. In Section 2 we present the Discrete Element model and the main assumptions of our modelling approach. We briefly describe in Section 3 the effects of explosions on targets and the model used to apply the loading on the masonry structure. We perform in Section 4 numerical tests of the response of a masonry wall subjected to far-field explosions, assuming (elastic) deformable masonry blocks. The results are compared and validated with existing experimental tests. In Section 5 we investigate the validity and accuracy of a rigid block model to predict the out-of-plane response of a masonry wall.

2 DISCRETE ELEMENT METHOD AND MODELLING ASSUMPTIONS

The Discrete Element Method is used to investigate the dynamics of masonry structures subjected to blast loading. The model allows to directly access the various micro-mechanical parameters, such as the constitutive behaviour of the interfaces and bricks, as well as the geometry of the building blocks. Furthermore, a discrete approach allows to simulate the progressive failure of masonry and capture with increased fidelity the post-peak, softening, dynamic behaviour of a masonry structure with bricks undergoing large displacements and rotations.

The DEM simulations are herein carried out by means of the 3DEC software [19]. A central finite differences scheme is used in this code for integrating in time the equations of motion of each block. This code provides the means to apply the conceptual model of a masonry structure as a system of blocks, either rigid or deformable. Block deformability is considered through internal discretization of blocks into finite differences. Herein deformable blocks are used to achieve a detailed description of the structural response. The validity of a rigid blocks modelling assumption is further investigated in Section 5.

A soft-contact algorithm is used to model the interactions between neighbouring blocks through interfaces/joints.

2.1 Elastic behaviour of the interfaces

A Discrete Element (DE) model with deformable blocks consists of deformable units which are subdivided into a finite-difference mesh of triangular elements, interacting along zero-thickness joints.

The elastic behaviour of the interfaces is defined through the following stress-displacement relationship [19]

$$\begin{pmatrix} t_n \\ t_t \end{pmatrix} = \begin{pmatrix} k_n & 0 \\ 0 & k_t \end{pmatrix} \begin{pmatrix} u_n \\ u_t \end{pmatrix} \quad \text{or} \quad \mathbf{t} = \mathbf{k} \mathbf{u}, \quad (1)$$

where \mathbf{t} and \mathbf{u} are the vectors collecting the normal, t_n , and tangential, t_t , forces per joint's unit area and the joint normal, u_n , and tangential, u_t , displacement, respectively. The elastic stiffness matrix \mathbf{k} collects the normal and tangential to the interface stiffnesses: k_n and k_t , respectively.

Normal and tangential stiffnesses can be computed from the properties of the masonry components (bricks and joints), considering the expansion in dimension of the masonry blocks and the soft-contact assumption. The identification of the numerical values of the elastic parameters is obtained assuming a stack bond masonry and uniform stress distributions both in the block and mortar, see Figure 1. The joint normal stiffness k_n is computed by requiring the analogy between a real masonry prism and the discrete element model, in terms of series of axial springs. The equivalent stiffness for the masonry prism in Figure 1 is

$$k_{n,eq}^{-1} = \left(\frac{E_b}{h_b}\right)^{-1} + \left(\frac{E_m}{h_m}\right)^{-1} \rightarrow k_{n,eq} = \frac{E_b E_m}{E_m h_b + E_b h_m} \quad (2)$$

with E_b , E_m the Young's moduli of the brick and the joint, respectively, and h_b , h_m the height of the block and the joint (masonry prism).

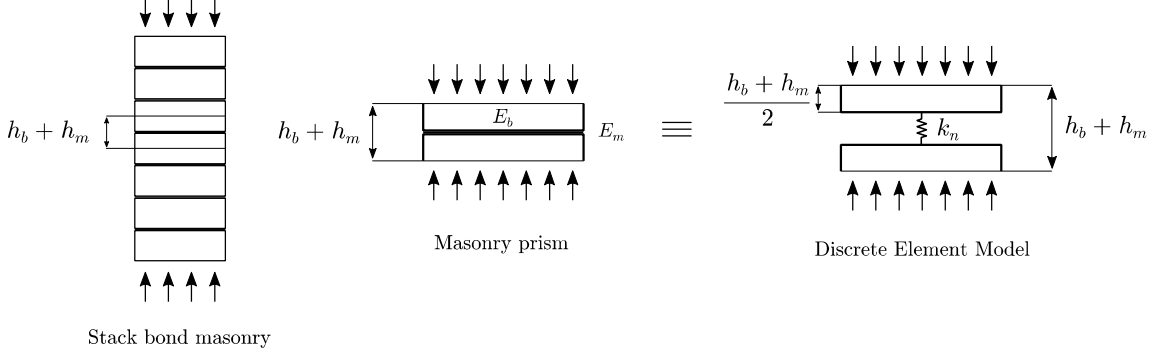


Figure 1. Scheme to determine joint normal stiffness. The value of k_n is found by requiring the equivalence between the axial stiffness of the real masonry prism (left) and the one of the DEM with expanded blocks and zero-thickness interfaces (right).

The Young's and shear moduli of deformable blocks, E^*_b and G^*_b , are modified to account for the expansion in dimensions (with respect to the real dimensions of the masonry bricks)

$$E^*_b = E_b \left(1 + \frac{h_m}{h_b}\right), \quad G^*_b = G_b \left(1 + \frac{h_m}{h_b}\right), \quad (3)$$

where G_b is the shear modulus of the masonry bricks. Equating expression (2) with the equivalent stiffness of the DE model along the normal direction, i.e., $k_{n,DE} = (h_b + h_m)/E^*_b$, we recover the joint normal stiffness $k_n = E_m/h_m$, and similarly, along the tangential direction, the tangential stiffness is computed as $k_t = G_m/h_m$.

2.2 Plastic and softening behaviour of the interfaces

In the absence of more detailed experimental data regarding the constitutive behaviour of masonry joints the Coulomb criterion seems to be a reasonable choice. Several experimental observations (e.g. [20-22]) justify its use up to moderate compression. Herein we assume an infinite compressive strength of the interfaces. Such hypothesis is verified a posteriori by monitoring the compressive stresses during each computation.

The maximum shear (or tangential) force per joint's unit area t_t (in N/m²) is limited by the Coulomb failure surface:

$$f_1 = t_t - c - t_n \tan \varphi \leq 0 \quad (4)$$

where c is the cohesion of the interface and φ the friction angle. Compression is here considered negative. In shear/tensional regime a tension cut-off is often used as shown in Figure 2. In other words, the maximum normal force per joint's unit area t_n (in N/m²) is limited by the tensile strength according to:

$$f_2 = t_n - f_t \leq 0 \quad (5)$$

where f_t is the tensile strength of the interface. The joint forces F_t and F_n are related to the corresponding displacements by Hooke's law

$$F_t = A_j t_t, \quad F_n = A_j t_n \quad (6)$$

where A_j is the joint's area. The two inequalities (4, 5) define the elastic domain of a masonry interface. The evolution and contraction under combined shear and normal plastic deformation of the elastic domain can be considered in terms of the various micro-mechanisms related to progressive softening of the joint. According to experimental results on interfaces, a softening behaviour is observed as depicted in Figure 2. In this way cohesion,

maximum tensile strength, and friction and dilatancy angles can evolve from their initial values c ; f_t ; φ ; Ψ to some smaller residual values c_{res} ; $f_{t,res}$; φ_{res} ; Ψ_{res} . All these values can be determined by typical experimental tests on interfaces.

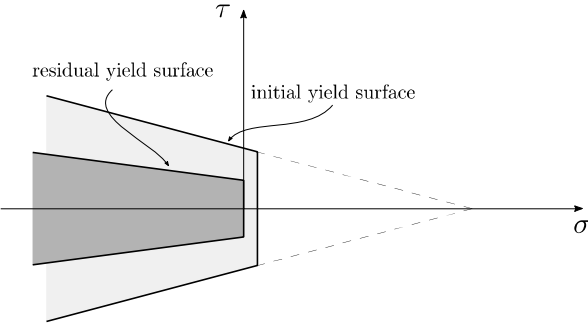


Figure 2. Initial and residual strength surfaces used for modelling joints behaviour.

Regarding the plastic flow rule, this is given by the following potentials:

$$g_1 = t_t - c - t_n \tan \Psi \quad (7)$$

$$g_2 = t_n - f_t \quad (8)$$

where Ψ is the dilatancy angle. If $\Psi = \varphi$ we say that the plastic flow rule is associative (normality condition), otherwise ($\Psi < \varphi$) the material obeys a non-associative plastic flow rule. In both cases, the following general relation between the rate of change of forces and the rate of change of total displacements stands

$$\dot{\mathbf{t}} = \mathbf{k}^p \dot{\mathbf{u}}, \quad (9)$$

with \mathbf{k}^p the plasticity matrix,

$$\mathbf{k}^p = \frac{k_n}{\kappa + \tan \varphi \tan \Psi} \begin{pmatrix} \tan \Psi & 1 \\ \tan \varphi \tan \Psi & \tan \varphi \end{pmatrix}, \quad (10)$$

where

$$\kappa = \frac{k_n}{k_t}, \quad (11)$$

$\dot{\mathbf{t}}$ and $\dot{\mathbf{u}}$ the vectors collecting the rate of change of the forces and of total displacement.

2.3 Constitutive behaviour of deformable blocks

An isotropic, elastic material behaviour is herein considered for the blocks. Infinite tensile and compressive strength are further assumed. This hypothesis may be strong in the case of relatively near-field explosions and especially in contact detonations, see e.g. [4]. Nevertheless, damage within the body of masonry bricks is generally negligible in far-field explosions, where the collapse of the masonry structure is governed by failure at the interfaces [1, 2, 4]. This is also corroborated by the fact that the tensile as well as the compressive strength are strain rate dependent. Extensive researches showed that at increasing loading rates the resistance of geomaterials, such as mortar, concrete, and marble, increases as well, mainly due to the finite growth rate of micro-cracks [23, 24] and the viscosity of the material [25]. At increasing strain rates, an increase of the tensile strength among other parameters, is observed. The dynamic increase factor for tensile strength for geomaterials (such as mortar, tuff, granite, etc.) usually varies between 1 and approximately 7 in function of the involved strain rates, see e.g. [26, 27].

In each computation, stresses as well as strain rates are monitored to verify that the related dynamic strength of the material is such that failure within blocks does not occur.

3 BLAST LOADS AND MODELLING

Explosion produces a blast wave of high-pressure accompanying high-temperature and supersonic expansion of gases. The abrupt increase of the pressure carried by a blast wave can produce severe structural damage. When the primary shock meets a target, it generates on it the so-called reflected overpressure, P_r , which is the difference between the pressure determined by the explosion increased by the reflection at target's surface and the ambient one, P_o . Figure 3 shows the schematic time variation of P_r , which is determined by the arrival time of the shock wave, t_A , the overpressure peak, P_{ro} , the positive phase duration, t_o , negative phase duration, t_{o-} , and the underpressure peak, P_{ro-} . These parameters are functions of the distance R and the explosive weight (conventionally expressed in TNT equivalent).

The pressure acting on a target due to blast loading is the algebraic sum of the hydrostatic overpressure and the dynamic pressure $C_D q := \rho u |u| / 2$, with C_D the drag coefficient (function of the target shape and Mach and Reynold numbers), ρ the density, and u the velocity of gas particles.

The simulation of a blast can be conducted by using different approaches [28-30]. Herein we refer to empirical models based on experimental results available in the existing literature.

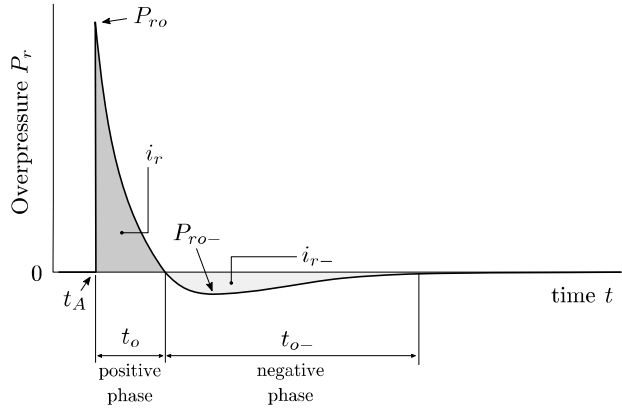


Figure 3. Time evolution of overpressure (i.e. the pressure measured relatively to the atmospheric one) due to an explosion acting on a target.

3.1 Blast model

We model blast actions following the work of Hyde [31] with the empirical model ConWep, which relies on the best-fit interpolations of the experimental results from Kingery and Bulmash [32]. The interpolations allow to determine the blast parameters and pressure loading from the knowledge of the trinitrotoluene (TNT) equivalent explosive weight, W , and the stand-off distance, R . The time evolution of the reflected pressure is modelled with the well-established modified Friedlander equation,

$$P_r(t) = P_{ro} \left(1 - \frac{t}{t_o} \right) \exp \left(-d \frac{t}{t_o} \right), \quad (12)$$

where d is the exponential decay coefficient. The impulse associated to the positive, i_{r+} , and the negative phase, i_{r-} , reads

$$i_{r+} = \int_0^{t_o} P_r(t) dt = \left(e^{-d} + d - 1 \right) \frac{P_{ro} t_o}{d^2}, \quad (13)$$

$$i_{r-} = \int_{t_o}^{\infty} P_r(t) dt = \frac{P_{ro} t_o}{d^2} e^{-d}, \quad (14)$$

respectively. Equation 16 allows to determine the exponential decay coefficient, d , by equating it with the best-fit interpolation of i_{r+} from experiments [32].

4 COMPARISON WITH EXPERIMENTAL TESTS

The proposed numerical model is herein compared and validated with existing experimental tests. Among the experiments available in the literature, we select one of the most well-documented [4]. Notice that performing blast experiments either in reduced or in full scale presents many difficulties, due to the nature of the loading action which may result in large uncertainties of the obtained results.

Michaloudis and Gebbeken [4] analyse the response of unreinforced masonry walls subjected to far-field and contact explosions through experimental and numerical investigations. Among four tests, two involve masonry walls subjected to the explosion of $W_1 = 810$ kg and $W_2 = 1150$ kg of TNT at $R = 37$ m from the targets. Due to the large stand-off distance, the blast wave impinges almost uniformly and instantaneously the target. However, no information is given concerning the evolution of the blast pressure in the experimental tests.

The brickwork consists of a running bond with bricks of nominal dimensions $a \times b \times w = 80 \times 240 \times 120$ mm, see Figure 4. The boundaries of the walls are constrained, through mortar interfaces, to stiff fixed supports.

In Test 1 ($W_1 = 810$ kg, $R = 37$ m), the observed maximum outward and inward deflection at the centre of the wall are 77 mm and 37 mm, respectively. In Test 2 ($W_2 = 1150$ kg, $R = 37$ m), a breach at the centre of the wall originates mostly only due to the damage of the joints. Failure within the body of individual bricks is not observed or is negligible [4]. The maximum dimensions of the breach are equal to 4 bricks along the length of the wall and to 13 bricks along the height.

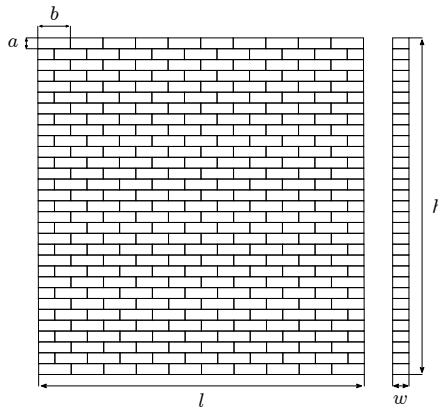


Figure 4. Geometrical model for test 1 and 2 in [4]. The masonry wall has thickness $w = 120$ mm and coursing consisting of a running brick bond. Bricks have nominal size $a \times b \times w = 80 \times 240 \times 120$ mm.

In the numerical DE model, a constant thickness of the mortar $h_m = 10$ mm is assumed in the lack of more detailed information for the walls. Table 1 presents the numerical material parameters which have been selected from the literature, see e.g. [17, 32, 33]. Superscripts h and b refers to head and bed joints, respectively. Subscript res identifies the residual (softening) value of the parameters, when differ from the initial ones (see Fig. 2). In the lack of information about the boundary conditions acting on the structure, the wall is considered simply supported at its four extremities, as complete rotational restraint or freedom may be difficult to achieve in practice. Blast loads are computed and applied with the dynamic library presented in Section 3.

Convergence analyses for contact and finite difference discretization are performed with the same criterion used in [34]. Two different loads are applied in two stages. First, a gravity load is applied, and the system is left to reach equilibrium. Second, increasing out-of-plane forces, proportional to the block mass, are applied to each block, up to wall failure. Due to the inherent, dynamic character of most DEM codes, including 3DEC, care was taken in order to assure quasi-static conditions until failure. The loads are applied adequately slow in order to assure a small ratio of the kinetic energy over the total energy of the system.

As far it concerns the specific DEM code used herein, 3DEC, the number of contact points situated across the wall thickness has a direct impact on the model response. This is especially important for out-of-plane loads as the one resulting from an explosion. From the convergence analyses, we find that at least 10 contact points are required to accurately modelling the out-of-plane deflection of the wall under study. The finite difference mesh for deformable blocks consists of tetrahedra with average characteristic length equal to 30 mm.

As follows, the numerical simulations consist of two stages. A gravity load is first applied assuming a linear elastic behaviour, then, once the system has reached the equilibrium, blast loads are applied. In order to model the fast-dynamic response of the structure, no mechanical damping formulation is used.

4.1 Test 1

Table 2 shows the results obtained with the DEM model for Test 1 ($W_1 = 810 \text{ kg}$, $R = 37 \text{ m}$) and compare them with the test data and the numerical computations presented in [4], which rely on similar modelling assumptions. The agreement of the results of the proposed model with the observed deflections is remarkably good (also compared to the numerical results in [4]). The maximum outward and inward displacements deviate from the experimentally observed one by 1.5 % and 3.2 %, respectively.

We present in Figure 5 the evolution in time of the numerically measured deflection at the centre of the wall. In the free-oscillating response, the system gradually dissipate energy as a result of the slippage along interfaces, until it reaches an equilibrium. The centre of the wall displays a permanent deflection of approximately 7.1 mm along the outward direction.

Blocks properties		Joint properties									
E_b^*	(MPa)	5220	k_n	(GPa/m)	50.0	c	(kPa)	500	φ	(°)	30
G_b^*	(MPa)	2170	k_t	(GPa/m)	20.83	c_{res}	(kPa)	0	ψ	(°)	0
density	(kg/m ³)	2470				f_t	(kPa)	100			
						f_{res}	(kPa)	0			

Table 1: Material parameters used in the numerical simulations with deformable DE.

The assumption of infinite strength of the blocks in compression/tension and of the interfaces in compression is verified *a posteriori*. In both cases (blocks and interfaces), stresses are found to be 60 % lower than the corresponding material strength.

Maximum deflection	Experiment	Numerical predictions		Relative error	
		DEM	from [4]	DEM	from [4]
Outward (mm)	77.0	78.2	56.3	1.5 %	26.8 %
Inward (mm)	37.0	38.2	13.4	3.2 %	63.7 %

Table 2: Comparison of the maximum outward and inward deflection at the centre of the wall for Test 1 ($W_1 = 810 \text{ kg}$, $R = 37 \text{ m}$) between the experimental values and the numerical predictions using deformable blocks (DEM) and the values obtained in [4].

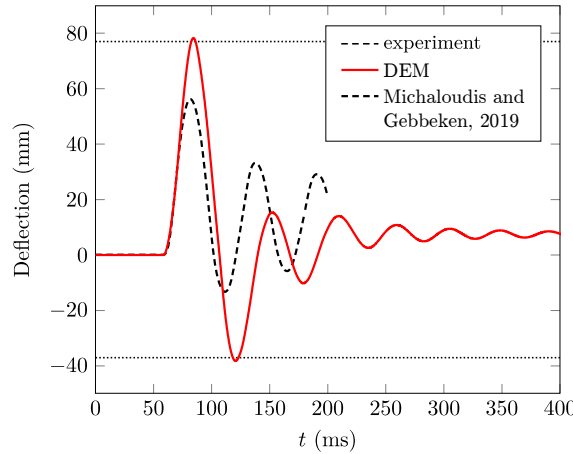


Figure 5. Evolution of the deflection at the centre of the wall for Test 1 ($W_1 = 810 \text{ kg}$, $R = 37 \text{ m}$) computed by the proposed DE model and from the computations in [4].

4.2 Test 2

We present in Figure 6 the response of the wall from the numerical DEM simulations of Test 2 ($W_2 = 1150 \text{ kg}$, $R = 37 \text{ m}$). The out-of-plane dynamic response and the consequent formation of the breach can be clearly observed.

Table 3 compares the dimensions of the breach from the experimental evidence and the numerical results. In Figure 7, we compare the final state of the masonry wall with a representative scheme obtained from the test results, see [4]. The DE model is found to well captures the form of failure, as well as the extension in height of the breach. However, less bricks are involved along the width direction. The number of bricks that travel from the wall is 22, while in the experiment is approximately equal to 40. The slight difference may be due to the complex fluid-structure interaction phenomena that take place, in the reality, as the breach originates. The blast pressure, acting continuously on the openings, may be the cause of a larger breach in the width, i.e., along the direction where the masonry brick are more likely to rotate. Furthermore, it is worth stressing that, in the test, some bricks involved in the breach, even if few in number, undergo damage, which is not considered in our model.

As for test 1, the assumptions of infinite compression strength of blocks and infinite tensile strength of blocks and interfaces are a posteriori verified. The compression stresses are both in the masonry bricks and the interfaces below the material strength [27]. Tensile stresses exceed in some bricks the material strength. Nevertheless, the enhancement in tensile strength due to high loading rates requires to be accounted for [26, 27]. The numerically measured strain rates within discrete elements are approximately $5\text{--}10 \text{ s}^{-1}$, which correspond to a dynamic tensile strength of approximately $4.5\text{--}6 \text{ MPa}$ [26, 27]. Only some bricks involved in the formation of the breach are subjected to tensile stresses as high as 5 MPa.

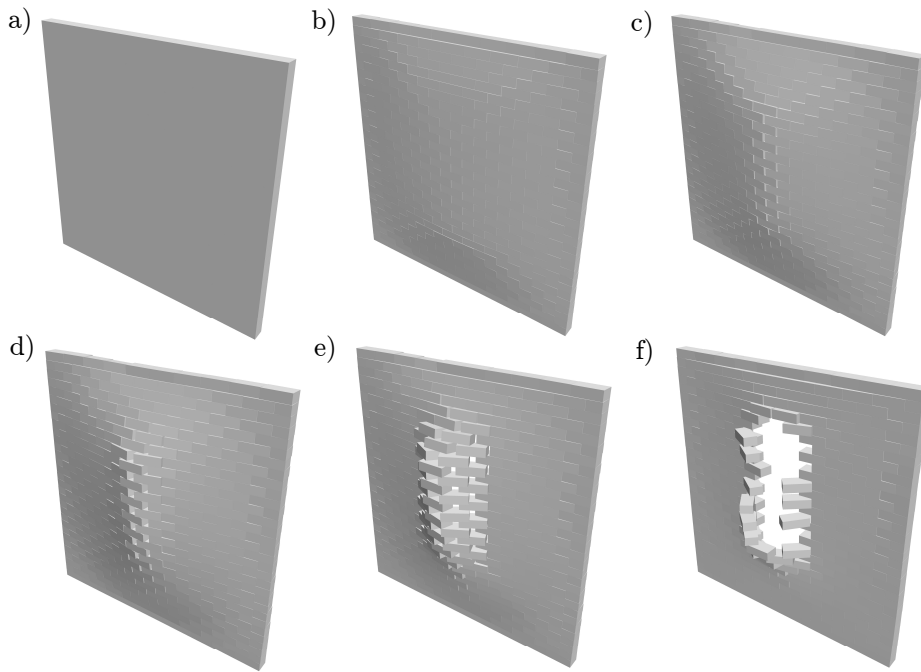


Figure 6. Response of the DE model for Test 2 ($W_2 = 1150 \text{ kg}$, $R = 37 \text{ m}$), a-e), and final state of the masonry wall, f).

Breach	Experimental	Numerical predictions	
		DEM	from [4]
Dimensions	13×4	14×2	14×3
No. of involved bricks	40	22	30

Table 3: Comparison of the dimensions of the breach for Test 2 ($W_2 = 1150 \text{ kg}$, $R = 37 \text{ m}$) experimentally observed and from the numerical predictions using deformable blocks (DEM) and the values obtained in [4].

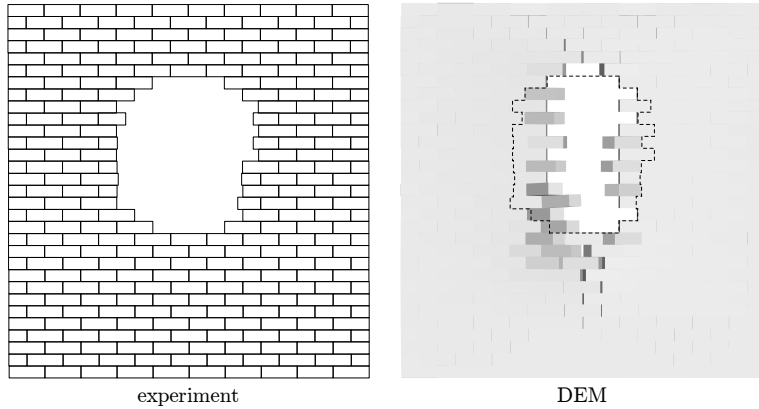


Figure 7. Comparison between the numerical DEM results (right) and the experiment (left) for Test 2 ($W_2 = 1150$ kg, $R = 37$ m). The experimental breach extension is schematically represented by the black dashed line.

The proposed DE model shows a good agreement with the tests both for the dynamic response (Test 1) and the form of the failure (Test 2). This is a key aspect that is necessary to consider in every numerical strategy and approach which may be used to investigate the response and failure modes of masonry structures, and in particular when the effects of blast loading are considered. A correct evaluation of the formation of breaches and weak planes may allow, through further investigations, the design of effective protections.

4.3 Effects of the (non-)associativity of the sliding behaviour of masonry joints

In the above calculations, a non-dilatant sliding behaviour was assumed for the interfaces, and namely $\psi = 0^\circ$, as usually displayed by masonry joints, see e.g. [21]. We investigate herein the effect of an associative behaviour of the interfaces, i.e. when $\psi = \varphi = 35^\circ$, on the response of the wall for both tests (1 and 2). All material parameters, except dilatancy, are kept the same as in Table 1.

Figure 8 displays the time evolution of the deflection at the centre of the wall for dilatant and non-dilatant joints. The associative case shows reduced out-of-plane response and increased strength, see also [35].

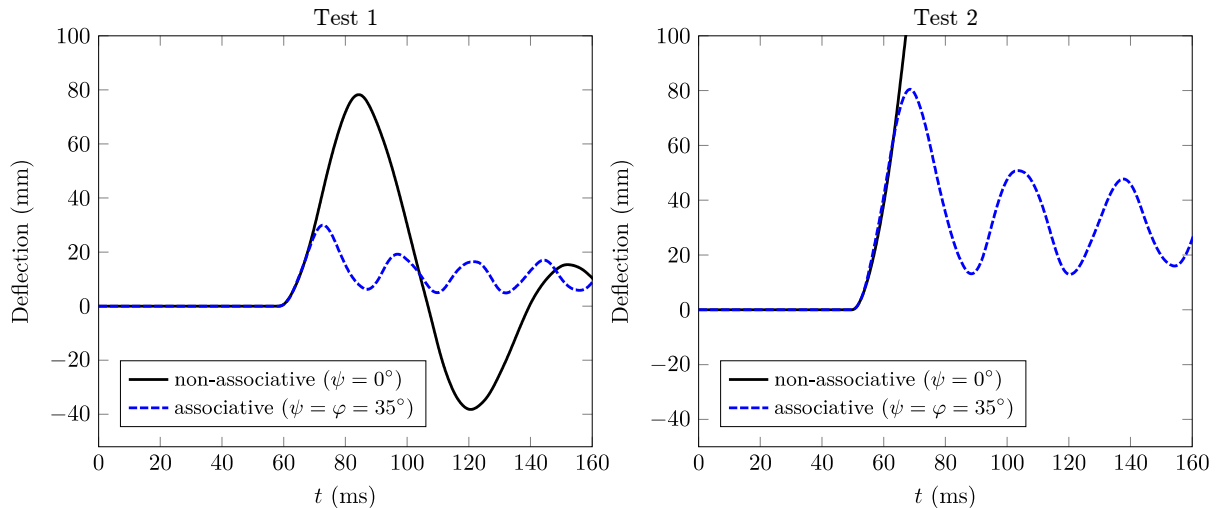


Figure 8. Influence of the dilatant behaviour of masonry joints in terms of the deflection at the centre of the wall for Test 1 ($W_1 = 810$ kg, $R = 37$ m), left, and Test 2 ($W_2 = 1150$ kg, $R = 37$ m), right.

In Test 1, the maximum deflection is 22.9 mm, namely 3.4 times smaller the one obtained with $\psi = 0^\circ$ (i.e. 78.2 mm). The maximum and minimum principal stress within masonry bricks are respectively 4 and 15 times larger than the values obtained with zero dilatancy. In Test 2, associativity of the interfaces results in a structure able to withstand the blast loading of 1150 kg of TNT. In this case, the maximum deflection is 80.5 mm, which is comparable to the results obtained with a non-dilatant behaviour, but under an explosive charge 340 kg smaller, i.e. 810 kg (Test 1).

5 IS A RIGID BLOCKS ASSUMPTION APPROPRIATE TO MODEL THE OUT-OF-PLANE RESPONSE?

Once the DE model has been validated with existing experimental results involving explosions, we investigate the simplified modelling assumption of infinitely rigid blocks which is often preferred in the literature, see e.g. [35-37], for its reduced computational cost with respect to the more detailed model with deformable blocks. A rigid blocks assumption is usually reasonable under relatively low compressive loads, where the deformation is principally concentrated at the interfaces [17]. Moreover, from an energetic approach, the assumption of rigid blocks is supposed to provide safe estimations (lower bound) of the overall strength. Nevertheless, masonry structures subjected to out-of-plane loading, as it is the case with the experiments herein considered [4] and as frequently occurs with explosive loads, the rigid blocks assumption can give unsatisfactory results, see e.g. [15].

Notice that several contact points through the thickness of the masonry structure undergoing out-of-plane displacement are required both with rigid and deformable blocks formulations, for more we refer to [35, 38, 39]. However, in a rigid block model, the stress distribution at the interfaces follows a linear diagram, as the faces remain planar, thus an accurate discretization of contacts is crucial. For instance, it has been proved that in the frame of the DEM code herein used, 3DEC, at least 3 contact points along the thickness are required to obtain an accurate representation of the bending stiffness [39].

With rigid blocks, the normal and tangential stiffnesses of the interfaces are appropriately modified with respect to the expressions previously derived. In this case, the stiffness of the entire system is reduced to the stiffness of the zero-thickness interfaces, k_n , and namely

$$k_n = \frac{E_b E_m}{E_m h_b + E_b h_m} \quad (15)$$

A similar expression can be derived for joint tangential stiffness k_t :

$$k_t = \frac{G_b G_m}{G_m h_b + G_b h_m} \quad (16)$$

with G_b and G_m the shear moduli of the masonry bricks and the mortar, respectively. The material parameters that define the plasticity behaviour and the corresponding softening remained unchanged, see Sect. 2. We present in Table 4 the material parameters used in the numerical DE model, derived from those given in Table 1 (for deformable DE) and considering the non-deformability of the blocks, see Eq.s (15) and (16). The discretization of the contact interfaces is investigated as presented in Section 4. From the convergence analyses, a discretization consisting of 20 contact points along the wall thickness is selected. Boundary conditions are kept the same as for the deformable DE.

As follows, we investigate the effects of the non-deformability of blocks in the numerical DE model. This is first accomplished in quasi-static conditions, applying a constant out-of-plane pressure to a localized region of the structure. Second, the dynamic response to blast loading is studied by numerical simulations of tests 1 and 2.

Blocks properties		Joint properties									
density	(kg/m ³)	2470	k_n^b	(GPa/m)	29.4	c	(kPa)	500	φ	(°)	30
			k_t^b	(Gpa/m)	12.3	c_{res}	(kPa)	0	ψ	(°)	0
			k_n^h	(Gpa/m)	15.2	f_t	(kPa)	100			
			k_t^h	(Gpa/m)	6.3	f_{res}	(kPa)	0			

Table 4: Material parameters used in the numerical simulations with rigid DE. Superscripts b and h refer to bed and head joints, respectively. The joints stiffnesses are differentiated along the two directions in order to consider the different height of masonry bricks, see Eq.s (15) and (16).

5.1 Response under quasi-static loading

A constant uniform pressure, $P = 100$ kPa, is applied to a centred region of the wall, 7 courses high and $3\frac{1}{2}$ wide. We assume a linear elastic behaviour of the interfaces. We present in Figure 8 the deformed shaped obtained with rigid DE and deformable ones. Table 5 compares the strain energies and maximum deflection obtained with the two models. Rigid blocks are found to underestimate the overall out-of-plane deflection with a maximum displacement equal to 1.55 mm with respect to the one predicted with deformable blocks, i.e., 2.26 mm. The reason lies on an intrinsic rotational locking (term we select in analogy with the well-known shear locking phenomenon observed in Finite Element Method formulations). The rotational locking happens independently from the fineness of the contact discretization, as the rigid block model consists of 20 contact points along the wall thickness. This is clearly shown in Figure 9 by the different slopes at the boundaries ($x = \pm 1.2$ m and $y = \pm 1.24$ m) for rigid and deformable DE.

Referring to Table 5, we notice that the overall (material) strain energy, blocks plus interfaces, is almost equal for both models, however, the contributions of the joints strain energy highly differ. In particular, the compressive and tensile strain energies with rigid DE are found to be approximately two times larger than with deformable blocks. This is a direct consequence of the inadequacy of a rigid body behaviour for the case where relatively high compressive forces develop. In the flexural response of the wall, the (deformable) blocks can deform significantly, phenomenon that is not capture by a rigid body model. Moreover, it should be noticed that in the specific DEM code used herein, the modelling assumption of interfaces represented by only two elastic parameters, namely normal and tangential stiffnesses, may cause the enhancement of the observed rotational locking with rigid blocks.

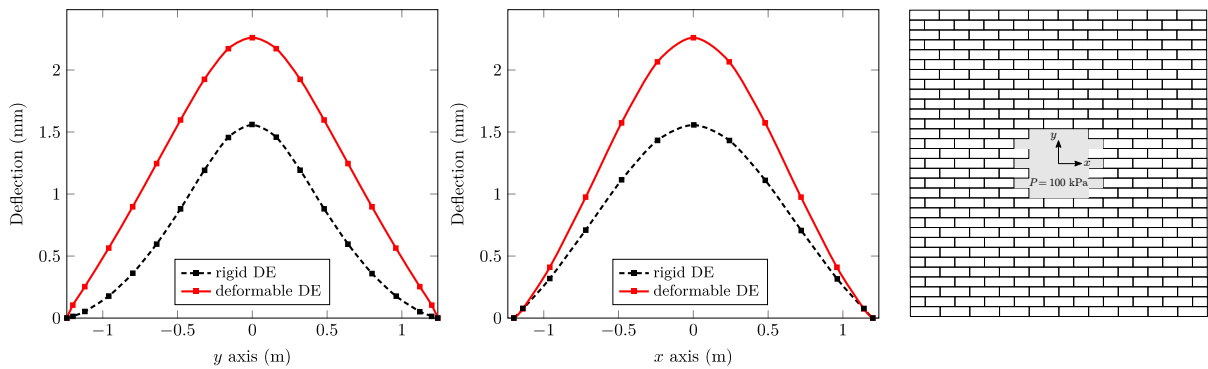


Figure 9. Comparison between rigid and deformable block models in terms of deflection along vertical (y axis) direction (left) and horizontal (x axis) direction (center). The curves are obtained by interpolation of the out-of-plane displacement of the centroid of blocks (marks). The constant and uniform pressure load is applied to the region highlighted in gray (right).

	Maximum deflection (mm)	Material strain energy (J)	Blocks strain energy (J)	Joints strain energy			
				shear (J)	compressive (J)	tensile (J)	total (J)
deformable DE	2.26	24.0	6.41	10.4	3.5	3.6	18.0
rigid DE	1.55	23.0	0.0	9.0	6.9	7.0	23.0
rigid/ deformable DE	71.9 %	96 %	0 %	86 %	197 %	194 %	127 %

Table 5: Comparison of the results from the models with rigid and deformable blocks under quasi-static conditions. Material strain energy refers to the algebraic sum of the joints and blocks strain energies.

5.2 Response under fast-dynamic excitations

The dynamic response of the same model used in Section 4 and derived from the experimental tests in [4] is herein investigated using the hypothesis of infinitely rigid blocks.

We compare in Table 5 the numerical predictions for Test 1 ($W_1 = 810$ kg, $R = 37$ m) using rigid DE with the deformable blocks model. The rigid DE model is found to underestimate the outward deflection by 37.1 % the experimentally measured value. A rather good agreement is found instead for the inward deflection.

We present in Figure 10 the time evolution of the out-of-plane displacement at the centre of the structure as computed with both DE models. It is worth noticing the difference of the mean value of the free-oscillating

response. Deformable blocks display a permanent deflection of approximately 7.1 mm in the outward direction. The rigid body model, instead, oscillates around a mean value equal to zero. The reason lies again on the rotational locking that a rigid DE description presents. The underestimated out-of-plane response results in a lesser amount of plastic energy dissipation at the interfaces.

Maximum deflection	Experimental	Numerical predictions		Relative error	
		rigid DE	deformable DE	rigid DE	deformable DE
Outward (mm)	77.0	48.4	78.2	37.1 %	1.5 %
Inward (mm)	37.0	39.2	38.2	5.6 %	3.2 %

Table 6: Comparison of the maximum outward and inward deflection at the centre of the wall for Test 1 ($W_1 = 810$ kg, $R = 37$ m) between the rigid and deformable block models and the experimental test.

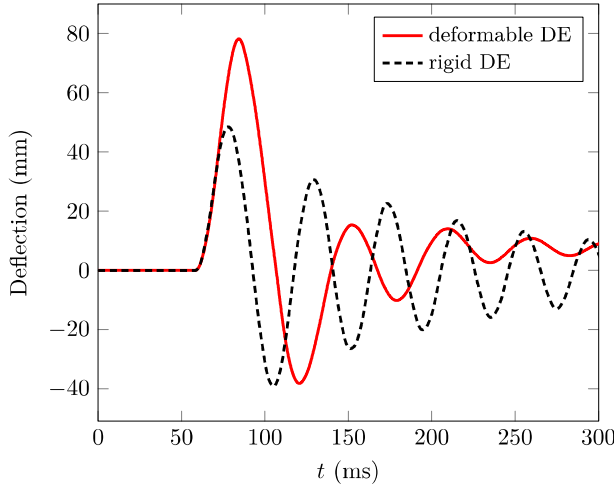


Figure 10. Evolution of the deflection at the center of the wall obtained from the numerical simulations with rigid and deformable DE for Test 1 ($W_1 = 810$ kg, $R = 37$ m).

In the case of Test 2 ($W_2 = 1150$ kg, $R = 37$ m), the rigid body model overall predicts the dimensions of the breach with good agreement with respect to the test results, see Figure 11. In particular, the width (4 courses of bricks) is accurately predicted by the numerical simulations, while the extension in height is overestimated, see Table 7. In this case, still due to the observed rotational locking, the rigid block model is found to overestimate the breach dimension, see Fig. 11.

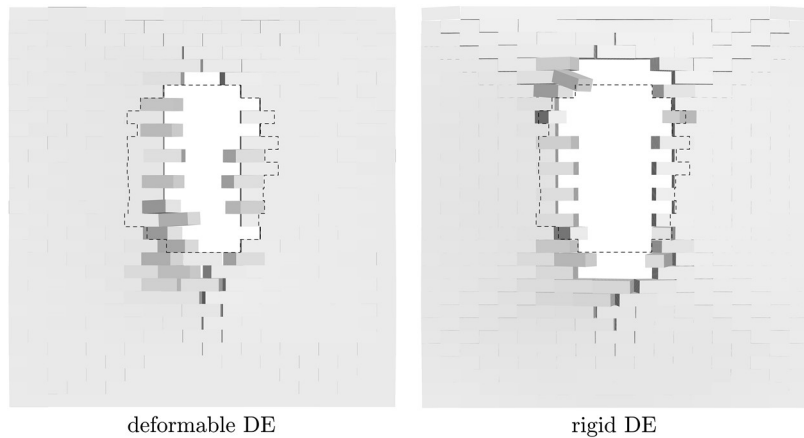


Figure 11. Comparison between the numerical results of the rigid and deformable block models for Test 2 ($W_2 = 1150$ kg, $R = 37$ m). The experimental breach extension is schematically represented by the dashed black line.

Breach	Experimental	Numerical predictions	
		deformable DE	rigid DE
Dimensions	13×4	14×2	18×4
No. of involved bricks	40	22	42

Table 3: Dimensions of the breach for Test 2 ($W_2 = 1150$ kg, $R = 37$ m). Comparison between the observed values and the numerical predictions using rigid and deformable blocks (DE).

6 CONCLUDING REMARKS

We investigated the dynamic response and failure of masonry structures subjected to blast loads. The Discrete Element Method (DEM) was herein proposed as an accurate and effective modelling strategy as it captures the progressive failure and response of a masonry structure with bricks undergoing large displacements and rotations. The proposed model relies on simplifying assumptions as it considers elastic deformable blocks and the non-linear material response as being limited to the mortar interfaces. Indeed, the mechanical behaviour of the joints plays a leading role in the overall strength and failure of the masonry structure under far-field explosions, while failure within the body of masonry bricks does not occur or is usually negligible [1, 2, 4, 17].

The accuracy of the DEM model and corresponding modelling assumptions were investigated and validated through comparisons with existing, well-documented experimental tests [4]. We proved that our numerical model can predict with high fidelity the dynamic response and failure under far-field explosions of masonry structures.

Once the numerical model was validated, it was used to assess the accuracy of a rigid block model in predicting the out-of-plane response under quasi-static and fast-dynamic conditions. The hypothesis of infinitely rigid blocks was found to overestimate the flexural stiffness of the system. As already discussed in [35, 38, 39], the contact discretization of the (rigid) Discrete Element (DE) model is a critical issue and has a direct impact on the model response. Nevertheless, the additional investigations we presented showed that, even in the case of a fine discretization of contacts, a rigid DE model displays an intrinsic rotational locking between adjacent blocks. This may result in a rather significant underestimation of the out-of-plane displacement of the structure, which was found to be around 70 % of the actual one (from experimental tests and a deformable block model) for the cases herein considered.

It is worth noticing however that a rigid block model has a reduced computational cost with respect to the more detailed description offered by deformable DE. In the simulations herein performed, the computing time for rigid blocks was approximately 50-60 % faster than with deformable ones.

Differently from the static and dynamic out-of-plane response, we found that the rigid block model gives sufficiently accurate predictions for the failure (strength) of the masonry structure subjected to blast loads.

The results obtained in this paper can be useful for improving the understanding on the behaviour of masonry structures under out-of-plane deformations and in particular under blast loads. Moreover, the proposed model can be used to perform reliable numerical tests of those systems for which the experimental set-up may be arduous and complex due to the fluid-structure interaction blast phenomena as well as the non-standard geometry of studied masonry structures [40], e.g. arches, vaults, domes, etc. This is a central point in the preservation of our architectural heritage against explosions as the numerical predictions of the failure modes can be used to design appropriate and effective protective devices. The proposed Discrete Element Method approach can be also a useful tool in investigating the response and strength of large masonry structures to blast loading with numerical methods based on continuum mechanics (upscaling/homogenization).

REFERENCES

- [1] Gagnet EM, Hoemann JM, Davidson JS (2017). Assessment of resistance definitions used for blast analysis of unreinforced masonry walls, International Journal of Protective Structures 8 (1), 125-151.
- [2] Keys RA, Clubley SK (2017). Experimental analysis of debris distribution of masonry panels subjected to long duration blast loading, Engineering Structures 130, 229-241.
- [3] Li Z, Chen L, Fang Q, Hao H, Zhang Y, Xiang H, Chen W, Yang S, Bao Q (2017). Experimental and numerical study of unreinforced clay brick masonry walls subjected to vented gas explosions, International Journal of Impact Engineering 104, 107-126.
- [4] Michaloudis G, Gebbeken N (2019). Modeling masonry walls under far-field and contact detonations, International Journal of Impact Engineering 123, 84-97.

- [5] Masi F, Stefanou I, Vannucci P, Maffi-Bertier V (2019). Response of monumental buildings to internal explosions. Proceedings of the 7th ECCOMAS Thematic Conference on Computational Methods in Structural Dynamics and Earthquake Engineering (COMPDYN 2019), Papadrakakis, Fraiadakis (eds), Crete, Greece, 24–26 June.
- [6] Masi F, Stefanou I, Vannucci P, Maffi-Bertier V (2019). Rocking response and overturning of museum artefacts due to blast loading. Proceedings of the 7th ECCOMAS Thematic Conference on Computational Methods in Structural Dynamics and Earthquake Engineering (COMPDYN 2019), Papadrakakis, Fraiadakis (eds), Crete, Greece, 24–26 June.
- [7] Gabrielsen B, Wilton C, Kaplan K (1975). Response of arching walls and debris from interior walls caused by blast loading, Tech. rep., URS Research Company, San Mateo, CA.
- [8] Varma RK, Tomar CPS, Parkash S, Sethi VS (1997). Damage to brick masonry panel walls under high explosive detonations, Pressure vessels and piping division. ASME 351, 207-216.
- [9] Dennis ST, Baylot JT, Woodson SC (2002). Response of 1/4-scale concrete masonry unit (CMU) walls to blast, Journal of Engineering Mechanics 128 (2), 134-142.
- [10] Abou-Zeid BM, El-Dakhakhni WW, Razaqpur AG, Foo S (2011). Response of arching unreinforced concrete masonry walls to blast loading, Journal of Structural Engineering 137 (10), 1205-1214.
- [11] Wang M, Hao H, Ding Y, Li ZX (2009). Prediction of fragment size and ejection distance of masonry wall under blast load using homogenized masonry material properties, International Journal of Impact Engineering 36 (6), 808-820.
- [12] Wei X, Stewart MG (2010). Model validation and parametric study on the blast response of unreinforced brick masonry walls, International Journal of Impact Engineering 37 (11), 1150-1159.
- [13] Macorini L, Izzuddin BA (2014). Nonlinear analysis of unreinforced masonry walls under blast loading using mesoscale partitioned modeling, Journal of Structural Engineering 140 (8), A4014002.
- [14] Rafsanjani SH, Lourenço PB, Peixinho N (2015). Implementation and validation of a strain rate dependent anisotropic continuum model for masonry, International Journal of Mechanical Sciences 104, 24-43.
- [15] Parisi F, Balestrieri C, Asprone D (2016). Blast resistance of tuff stone masonry walls, Engineering Structures 113, 233- 244.
- [16] Silva LC, Lourenço PB, Milani G (2017). Rigid block and spring homogenized model (HRBSM) for masonry subjected to impact and blast loading, International Journal of Impact Engineering 109, 14-28.
- [17] Stefanou I, Sab K, Heck JV (2015). Three dimensional homogenization of masonry structures with building blocks of finite strength: A closed form strength domain, International Journal of Solids and Structures 54, 258-270.
- [18] Draganić H Varevac D, Lukić S (2018) An overview of the methods for blast load testing and devices for pressure measurement, Advances in Civil Engineering, ID 3780482.
- [19] Itasca Consulting Group Inc. (2013), 3DEC 5.0, Minneapolis, MN 55401.
- [20] van der Pluijm, R (1999). Out-of-Plane bending of Masonry. Behavior and Strength, Technische Universiteit Eindhoven.
- [21] Lourenço PB, Ramos LF (2004). Characterization of cyclic behavior of dry masonry joints, Journal of Structural Engineering 130 (5), 779-786.
- [22] Vélez LFR, Magenes G, Griffith MC (2014). Dry stone masonry walls in bending—part I: Static tests, International Journal of Architectural Heritage 8 (1), 1-28.
- [23] Freund L (1972). Crack propagation in an elastic solid subjected to general loading—i. constant rate of extension, Journal of the Mechanics and Physics of Solids 20 (3), 129-140.
- [24] Freund L (1972). Crack propagation in an elastic solid subjected to general loading—ii. non-uniform rate of extension, Journal of the Mechanics and Physics of Solids 20 (3), 141-152.
- [25] Weerheim J (1992). Concrete under impact tensile loading and lateral compression, Ph.D. thesis, TU Delft, Delft University of Technology.
- [26] Chen X, Wu S, Zhou J (2014). Experimental study on dynamic tensile strength of cement mortar using split Hopkinson pressure bar technique, Journal of Materials in Civil Engineering 26 (6).
- [27] Ross CA, Tedesco JW, Kuennen ST (1995). Effects of strain rate on concrete strength, Materials Journal 92 (1), 37-47.
- [28] Remennikov AM (2003). A review of methods for predicting bomb blast effects on buildings, Journal of Battlefield Technology 6, 5-10.
- [29] Larcher M, Casadei F (2010). Explosions in Complex Geometries — A Comparison of Several Approaches, International Journal of Protective Structures 1 (2), 169-195.
- [30] Masi F, Stefanou I, Vannucci P (2018). A study on the effects of an explosion in the Pantheon of Rome, Engineering Structures 164, 259-273.
- [31] Hyde D (1993). Conwep: Conventional weapons effects program, US Army Engineer Waterways Experiment Station, USA.
- [32] Kingery CN, Bulmash G (1984). Air blast parameters from TNT spherical air burst and hemispherical burst,

- Tech. rep., U.S. Army Ballistic Research Laboratory.
- [33] Wild S, Gailius A, Hansen H, Pederson L, Szwabowski J (1997). Pozzolanic properties of a variety of European clay bricks, *Building Research & Information*, 25 (3), 170-175.
 - [34] Petry S, Beyer K (2015). Cyclic test data of six unreinforced masonry walls with different boundary condition, *Earthquake Spectra* 31 (4), 2469-2484.
 - [35] Godio G, Stefanou I, Sab K (2018). Effects of the dilatancy of joints and of the size of the building blocks on the mechanical behavior of masonry structures, *Meccanica* 53 (7), 1629-1643.
 - [36] Bui TT, Limam A (2012). Masonry walls under membrane or bending loading cases : experiments and discrete element analysis. Proceedings of the 11th International Conference on Computational Structures Technology, Dubrovnik, Croatia, 4–7 September.
 - [37] Çakt E, Saygl Ö, Lemos JV, Oliveira CS (2016). Discrete element modeling of a scaled masonry structure and its validation. *Engineering Structures* 126, 224–236.
 - [38] Lemos JV (2007). Numerical issues in the representation of masonry structural dynamics with discrete elements. Proceedings of the 1st ECCOMAS Thematic Conference on Computational Methods in Structural Dynamics and Earthquake Engineering (COMPDYN 2019), Papadrakakis, Fraiadakis (eds), Crete, Greece, 13–15 June.
 - [39] Lemos JV (2017). Contact representation in rigid block models of masonry, *International Journal of Masonry Research and Innovation* 2 (4), 321-334.
 - [40] Masi F, Stefanou I, Vannucci P, Maffi-Bertier V (2019). Masonry vaults under explosive loads. Proceedings of the 7th ECCOMAS Thematic Conference on Computational Methods in Structural Dynamics and Earthquake Engineering (COMPDYN 2019), Papadrakakis, Fraiadakis (eds), Crete, Greece, 24–26 June.